THE BALTIC JOURNAL
OF ROAD AND BRIDGE ENGINEERING

2010
5(3): 139–147

INVESTIGATION OF THE SAND POROSITY VIA OEDOMETRIC TESTING

Jonas Amšiejus[1], Rimantas Kačianauskas[2], Arnoldas Norkus[3], Liudas Tumonis[4]

[1, 3, 4]*Dept of Geotechnical Engineering, Vilnius Gediminas Technical University,*
Saulėtekio al. 11, 10223 Vilnius, Lithuania
E-mails: [1]ajonas@.vgtu.lt; [3]Arnoldas.Norkus@vgtu.lt; [4]Liudas.Tumonis@vgtu.lt
[2]*Dept of Strength of Materials, Vilnius Gediminas Technical University,*
Saulėtekio al.11, 10223 Vilnius, Lithuania
E-mail: Rimantas.Kacianauskas@vgtu.lt

Abstract. Investigation of the porosity of Klaipėda sand by oedometric test is presented. The Klaipėda sand is typical Baltic see-shore sand consisting of grains the average diameter of which varies from 1.18 mm to 0.3 mm. Variation of the porosity during oedometric compression of the whole mixture of the sand and of three separate fractions were investigated experimentally. Porosity was characterised by the maximal (initial) and minimal (after compression) values of the void ratio. It was proved experimentally that porosity of the sand mixture is practically predicted by the coarse-grained fraction with grain diameters ranging between 1.18 mm and 0.6 mm. The role of microstucture in the densification mechanism is explained by employing the discrete element method simulations. The spherical particles and commercial EDEM code were used for modelling purposes. Discrete element method simulations confirmed generally the macroscopic experimental results and yielded additional data on microscopic behaviour. The non-smooth deformation behaviour was observed during detailed numerical time-history analysis. The detected instabilities are explained by rearrangement of the sand grains.

Keywords: sand, oedometer test, void ratio, discrete element method (DEM), spherical particles.

1. Introduction

A proper understanding of the mechanical behaviour of soils is of the major importance in the construction engineering, including construction of bridges and roads. In major cases, the soil (i.e. a basement for engineering structures) is treated as a continuum. However, the non-conventional behaviour, i.e. the transient state of the soil varies between the liquid and deformable solid states. Rigid particles, voids between them that could be filled by water and/or gas are the main contributors, conditioning the state of stress and deformability properties of this complex mixture in whole.

The macroscopic behaviour of soil as homogeneous compressible continuum is described in terms of the internal state variables, namely, stresses, internal pressures, strains, displacements, velocities, and etc. The relationship between them is governed by the various models which are ranging from the simplified engineering approaches up to the sophisticated elastic-plastic-viscous theories. Description of them may be found in numerous textbooks, e.g. in Terzaghi *et al.* (1996), Ortigao (1995), Mitchell (1993), Fredlund and Rahardjo (1993).

Porosity (a parameter describing the void contribution to soil volume) variability is of a major importance when describing its deformability in stress ranges compatible with conventional design.

Verification of the soil models requires experimental evidence. In major cases, the physical and mechanical properties of soils are site-specific (Juknevičiūtė, Laurinavičius 2008; Ždankus, Stelmokaitis 2008). Therefore, usually the requested information on the soil properties is obtained for each construction site. This procedure is relatively expensive in both financial and time resources. Therefore, any approach (e.g. numerical simulation) minimizing the extent of field experiments for identifying soil mechanical properties is actually expected.

Recently the behaviour of soils has been extensively investigated via analytical, experimental and numerical approaches. It is worth to note that standard well defined testing procedures (Head 1986) have been developed for the experimental evaluation of the soil behaviour. The oedometric, the triaxial and the direct shear tests are at present the most common tests for determining the macroscopic soil parameters in laboratory (Amšiejus *et al.* 2009; Amšiejus, Dirgelienė 2007; Lade, Prabucki 1995; Lade, Wasif 1988; Peric, Su 2005; Vervečkaitė *et al.* 2007). The oedometric test is acknowledged to be the most wide-

ISSN 1822-427X print / ISSN 1822-4288 online
doi: 10.3846/bjrbe.2010.20
http://www.bjrbe.vgtu.lt

ly employed general method for evaluating the soil compressibility by measuring porosity changes vs. pressure.

Despite the huge effort, adequacy of theoretical models of the soils to reality is still problematic. Soils in general and sands in particular are of the discrete nature and present heterogeneous compositions of grains. The continuum approach used in a frame of the classical mechanics does not provide insight into variation of porosity occurring by the local motion at the scale of individual grain.

The experimental investigation of particle's interaction is quite costly, therefore, application of numerical simulations are frequently involved to enhance macroscopic physical experiments. The discrete (distinct) element method (DEM) became recognized as a tool for simulating the particulate matter after the publication of the work by Cundall and Strack (1979). The DEM concept offers a unique approach capturing the various particle shapes and physical models by a discrete set of the quantities. The fundamentals of DEM and the important details may be found in books and review papers of Allen and Tildesley (1987), Pöschel and Schwager (2004), Džiugys and Peters (2001), Kruggel-Emden *et al.* (2007), Zhu *et al.* (2007), Zhu *et al.* (2008).

Discrete concept and available commercial DEM codes like the *DEM Solutions, 2009. EDEM v2.2, Edinburgh, UK, DEM Solutions L; Itasca, 2003, PFC 3D User's manual, v3.0, Minneapolis, Minnesota, USA, Itasca Consulting Group Inc.* and numerous non-commercial research codes made DEM as an attractive research tool.

At the same time, computational capabilities limiting a number of particles remains the main disadvantages of the DEM technique. Simulation technique and software issues are discussed by Raji and Favier 2004, Balevičius *et al.* 2006, Kačianauskas *et al.* 2010.

This tool is efficient when simulating micro-scale response and explaining the physical nature of sand as composite discrete material.

Some applications of the DEM to modelling of dry sands may be emphasised. They comprise behaviour of sand in technological processes such as filling and compaction of sand by vibration (Rojek *et al.* 2005) or simulation of various tests. In many cases, three-dimensional sample in a form of rectangular parallelepiped was examined. The effect of the use of flat boundaries during one-dimensional compression was considered by Marketos and Bolton (2010). A cuboidal sample to simulate biaxial compression with rigid walls was studied by Yan *et al.* (2009). Similar approach in numerical simulations of the triaxial compression was employed by Belheine *et al.* (2009). DEM simulations of standard oedometric tests with cylindrical samples were presented by Oquendo *et al.* (2009).

The paper presents experimental investigation of the Klaipėda sand by oedometric test supported by the DEM simulations. It is organised as follows. An investigation concept and the basic data are given in section 2. Experimental set-up and testing results are given in section 3. The DEM methodology with particular emphasis on description of motion and inter-particle forces is presented in section 4. The simulation results and the discussion are given in section 5; conclusions are presented in section 6.

2. Porosity problem and basic data

The state analysis of soils requested for engineering application is much more difficult when compared to structural analysis. The deformation of the traditional construction material such as steel or concrete occurs without significant volume change because of relative material continuity. However, sand as the natural granular material possesses the considerable compressibility and is subjected to densification during deformation with a continuous change of volume. Therefore, investigation of porosity is the important step related to final evaluation of the stress-strain state of sand and its physical constants. It could be reminded, that densification of the sand layers predefines the settlements of the structures and evaluation of the porosity is compulsory in foundation design (Murthy 2002; Terzaghi *et al.* 1996).

Moreover, all the natural geological materials especially sands are characterised by diversity of the grains sizes and shapes, conditioning the actual physical and mechanical properties. Since the microstructure of soils is geologically site-specific, therefore, their properties should be tested for each general construction site.

The Klaipėda sand as typical Baltic see-shore sand is under investigation. Its mineralogical composition consists basically of dominating ingredients, namely, of ~ 85% silica and of ~ 6% sunstone with remaining contribution of carbonate, mica and some other minerals.

Composition of the Klaipėda sand was evaluated via standard granulometric testing according to *Geotechnical Investigation and Testing. Identification and Classification of Soil. Part 2: Principles for a Classification.* When considering the sand microstructure, it was found that the grains of sand are of a rounded shape, the grain surface is of abrade smooth character.

Average diameter d particles vary in the range from 1.18 mm to 0.3 mm. Size distribution of sand grains is presented in Fig. 1. The sand properties due to above mentioned standard are: uniformity coefficient $C_U = 1.47$, coefficient of curvature $C_C = 0.93$. The porosity in current

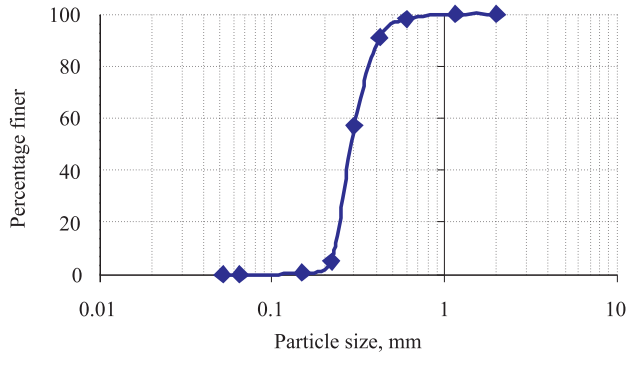

Fig. 1. Size distribution of Klaipėda sand grains

investigation is characterised by a void ratio e obtained as the ratio of voids volume to the volume of the grains V_{gr}, m^3, i.e.:

Finally, the void ratio is

$$e = \frac{V_{sol} - V_{gr}}{V_{gr}}, \quad (1)$$

where V_{sol} – the volume occupied by soil as solid material which is measured in oedometric device, m^3.

The current study is aimed not only to quantify max/min porosity of the dry virgin Klaipėda sand under uniaxial compression but also to explain the role of microstucture in the densification mechanism on the basis oedometric testing and employing the DEM simulations.

3. Experimental analysis by oedometric testing

3.1. Experimental set-up

The uniaxial oedometric compression tests have been carried out in standard manner following (Atkinson *et al.* 1997).

An oedometric testing device consists of a metallic cylinder being fixed to a rigid base (Fig. 2). The internal volume of the cylinder is of height H = 35 mm and diameter D = 70 mm. It responds to the volume of the sample of the soil. All cylinder walls are assumed to be rigid. The friction between the sample and the device walls is not eliminated.

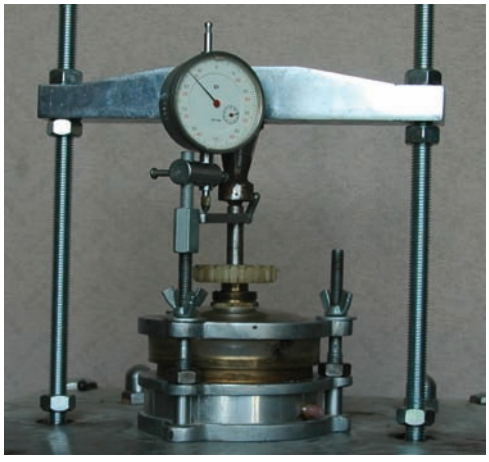

Fig. 2. Oedometric device

For the experimental procedures the sand was dried up and test samples have been prepared by the filling. Therewith, the grains were slowly poured into the cylinder of device. The top surface was flattened by removing horizontally the grains above the surface. Then, an initial vertical pressure (loading) was applied on the top wall by the rigid stamp. The loading was realized via the step-by-step procedure therewith each loading increment was imposed by a specified loading rate and kept constant after some time to relax a sample. The incremental loading was continued until the required final loading level has been reached.

The axial deformations were measured by the controlling the height decrease of the sample height Δh during the test.

Evaluation of void ratio e described via Eq (1) was done by having employed the following assumptions:

- the volume of sand grains remains constant $V_{gr} = const$, i.e. their volume changes due to contact deformation are negligibly small;
- the particles are homogeneuous and have the constant density of the grains ρ;
- the macroscopically observed volume changes of the specimen are specified by reduction of pores because of particle's rearrangement.

As a consequence of the first two assumptions, the volume of grains $V_{gr} = const$ could be calculated from the weight of the tested material.

The initial void ratio e_0 is characterised by its max value directly obtained by expression (1) assuming that entire volume of the cylinder is occupied by granular solid, i.e. $V_{sol} = V_{cyl}$.

At each load level i defined by pressure increment Δp, the porosity e_i is related to the measured height h change Δh_i of the specimen. It is calculated as follows

$$e_i = e_0 - \frac{\Delta h_i \left(1 + e_0\right)}{h}. \quad (2)$$

Oedometric modulus E_0 (explicitly employed in geotechnical engineering) can be obtained in the same manner by

$$E_{0i} = \frac{\Delta \sigma_{zi}}{\Delta e_i}\left(1 + e_0\right), \quad (3)$$

where $\Delta \sigma_{zi} = \Delta p_i$ and Δe_i – specimen axial stress and void ratio change, respectively.

3.2. Experimental results

Three samples denoted hereafter as Sample 1, Sample 2 and Sample 3 were prepared from three segregated fractions of the sand grains, namely, the coarse-grained fraction consisting of relatively large particles, varying in the range between 1.18 mm and 0.6 mm; the medium-grained fraction consisted of particles varying in the range between 0.6 mm and 0.425 mm and the fine-grained fraction consisted of relatively fine particles varying in the range small grains varying in the range between 0.425 mm and 0.3 mm were extracted and tested. Sample 4, the composition of all three fractions of equal parts, i.e. consisting of particles varying in the range within 1.18 mm and 0.3 mm, was also prepared and investigated in addition.

Each of the above mentioned samples were subjected by the identical loading history up to a max pressure magnitude p = 400 kPa (Fig. 3). The load was increased via the four loading steps specified by the equivalent pressure increment Δp_i = 100 kPa, ensuring the axial strain rate of 0.11 mm/min. The relaxation at each loading increment lasted 60 s.

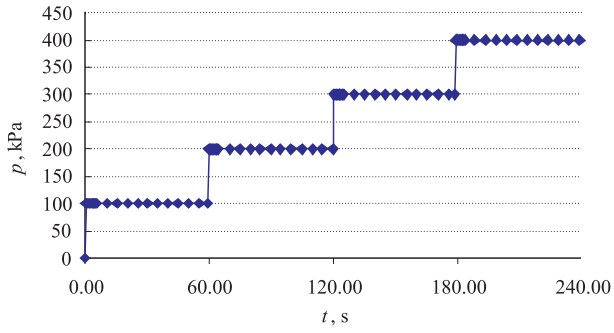

Fig. 3. Loading history for Samples 1–4

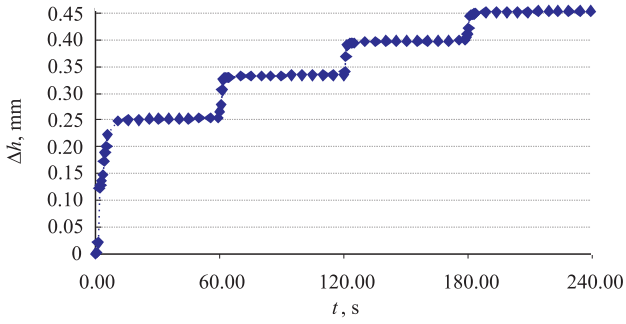

Fig. 4. Δ*h* vs. time during test process for Sample 1

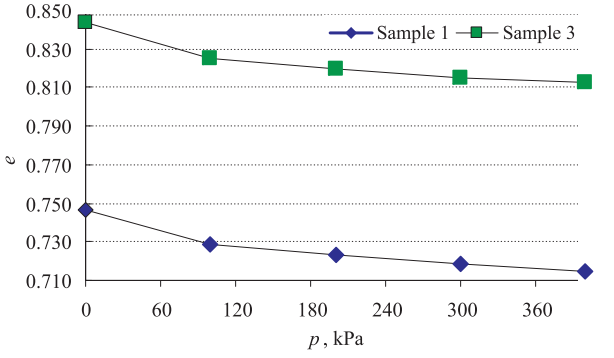

Fig. 5. Void ratio vs. loading for Sample 1 and 3

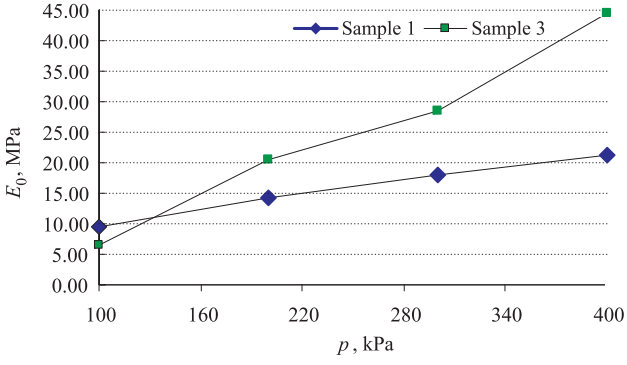

Fig. 6. Oedometric modulus vs. loading for Sample 1 and 3

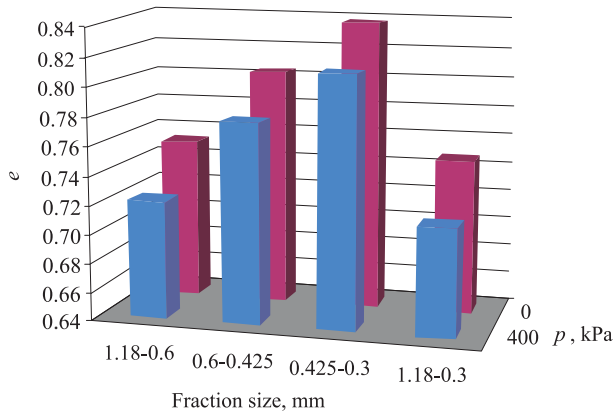

Fig. 7. Summary of experimental porosities: max and min void ratios of separate fractions and final mixture

The measured decrease of the height Δh of solid material, e.g. for Sample 1, during the testing is shown in Fig. 4.

For definition of the densification nature the graphs presenting variations of the void ratio *e* and oedometric modulus E_0 for various loading levels can be given. The above mentioned parameters obtained by expressions (2) and (3) on the basis of experimental results for Samples 1 and 3 given in Figs 5 and 6 for illustration.

The graphical summary of porosity results is illustrated in Fig. 7. The three-dimensional histogram represents the max (initial) and min (the end of test) values of the void ratio of segregated fractions (Samples 1–3) and that of mixture (Sample 4) of sand.

Results show that max porosity (e_{0m} = 0.844) as well as min porosity (e_{04} = 0.714) of the sand mixture (Sample 4) are practically predicted by the coarse-grained fraction (Sample 1).

4. DEM simulations

4.1. Theoretical background

The DEM methodology considered in this paper is aimed at simulating the dynamic behaviour of dry non-cohesive frictional visco-elastic particles. Sand sample is presented as a system of the finite number of particles which is synonymous to discrete elements. Each particle is treated as deformable body with the given geometry and material properties. As the particles move, they impact each other and undergo the contact deformations. The particle shape is restricted to spheres. The DEM methodology employed in below simulations is based on the original proposals of Cundall and Strack (1979) while an evaluation of some force components involves later developments of Tsuji *et al.* (1992), Raji and Favier (2004). The latter was implemented into the commercial code EDEM developed by DEM Solutions Ltd. (DEM Solutions 2009).

The DEM proceeds separately each particle denoted hereafter by a subscript *i*. The motion of the particle as a rigid body in the global Cartesian coordinates is described using a framework of classical mechanics. The translation-

al behaviour of arbitrary particle i is characterized by the global parameters: positions X_i, velocities $\dot{X}_i$ and accelerations $\ddot{X}_i$ of the mass centre; as well as the resultant force vector F_i acting on the particle. The motion of particle i in time t obeys the Newton's second law and is formulated for the mass centre of the particle as

$$m_i \ddot{X}_i(t) = F_i(t). \tag{4}$$

The equations describing the rotational motion depend on the shape of particle but for spheres they may be considered in the same way as translation. The rotation is governed by three independent rotational degrees of freedom $\theta_i(t)$ presenting Euler angles, angular velocities $w(t)$ and accelerations $\dot{w}(t)$. Finally, rotation equations related to global coordinates of particle are:

$$I_i \dot{w}_i = T_i, \tag{5}$$

where m_i – the mass, kg; I_i – the moment of inertia, of particle i, m^4. Vectors F_i and T_i present the resultant force and torque acting on the particle i. The gravity force and all contact forces between contacting neighbour particles will be taken into account.

Methodology of calculating contact forces and torques in (4–5) depends on the particle's size, shape and mechanical properties as well as on the constitutive model of the particle interaction.

Contact between the particles i and j will be considered to illustrate DEM methodology. Geometry of particles is defined by the radii R_i and R_j while elasticity properties by elasticity moduli and Poisson's ratios E_i and E_j, ν_i and ν_j, respectively. Interaction between colliding bodies is defined by the coefficient of restitution e end coefficient of friction μ.

The force and displacement vectors at the particle contact point of particles i and j can be separated into the normal and tangential components to the contact surface which are denoted hereafter by the superscripts n and t, respectively. The normal direction of the contact surface is defined by the unit vector n_{ij} extending through the centre of the contact area C_{ij}. The normal contact direction n_{ij} for the spherical particles always coincides with the line connecting the particle centres. The unit vector t_{ij} of the tangential contact direction is perpendicular to n_{ij}.

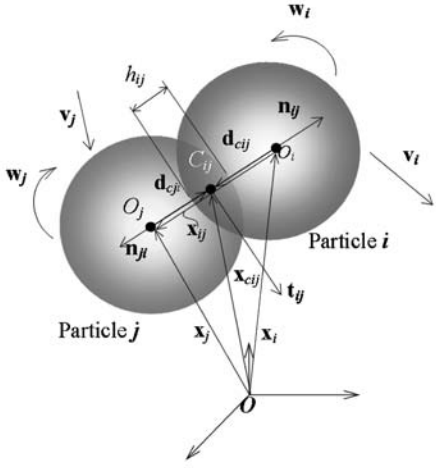

Fig. 8. Illustration of contact for spherical particles

The particle's deformation due to collision is assumed to be approximated by the overlap of the particles (Fig. 8). The depth of the overlap h_{ij} is considered as normal displacement component. It is provided that overlap is significantly smaller than the particle size, $h_{ij} << R_i, R_j$. The size of the overlap h_{ij} is defined by considering the distance between the centres of the spheres

$$h_{ij} = R_i + R_j - \left| X_i - X_j \right|. \tag{6}$$

During a contact, the particles move relatively to each other with velocity v_{ij}^t along the distance δ_{ij}^t in the tangential direction, termed hereafter as tangential displacement. It is obtained by integrating velocity as

$$\delta_{ij}^t = \left| \int v_{ij}^t(t) dt \right|. \tag{7}$$

Therewith, partial slip in the case, if the tangential force exceeds the limit defined by static friction is captured.

Decompose force vector $F_{ij,\,cont}$ into a normal and a tangential components by

$$F_{ij,\,\mathrm{cont}} = F_{ij}^n + F_{ij}^t. \tag{8}$$

Then both normal and tangential components present a combination of the elasticity, damping and separation or sliding effects. An inter-particle contact is defined by stiffness coefficients k_{ij}^n and k_{ij}^t, by the damping coefficients and η_{ij}^n and η_{ij}^t the friction coefficient μ, respectively.

The normal elasticity force F_{ij}^n follows Hertz model while damping force is defined by the Tsuji model (Tsuji *et al.* 1992). Explicitly, the normal force is expressed as

$$F_{ij}^n = k_{ij}^n (h_{ij})^{\frac{2}{3}} n_{ij} - \eta_{ij}^n (\dot{h}_{ij})^{\frac{1}{4}} n_{ij}, \tag{9}$$

where the normal stiffness parameter $k_{ij}^n = \frac{4}{3} E^{eff} \sqrt{R^{eff}}$ – related to the effective Young's modulus E^{eff} given by $\frac{1}{E^{eff}} = \frac{1-\nu_i^2}{E_i} + \frac{1-\nu_j^2}{E_j}$. The reduced particle radius R^{eff} is described by $\frac{1}{R^{eff}} = \frac{1}{R_i} + \frac{1}{R_j}$. The normal damping parameter $\eta_{ij}^n = \gamma^n m^{eff}$ is related to the effective mass m^{eff} given by $\frac{1}{m^{eff}} = \frac{1}{m_i} + \frac{1}{m_j}$, and to the normal damping parameter γ^n defined according to the Tsuji model, being related to the normal coefficient of restitution c^n.

The tangential force component F_{ij}^t reflects the static state prior to gross sliding or dynamic state after the gross

sliding. The static force $F^t_{ij,st}$ comprises elastic and viscous ingredients identical to those of normal force (9), while the dynamic force $F^t_{ij,dyn}$ confirms the friction force expressed by the Coulomb' low. The tangential force can't exceed the friction limit, the real force responds to the min of the two above forces:

$$F^t_{ij} = -t_{ij}\min(\left|F^t_{ij,st}\right|, \left|F^t_{ij,dyn}\right|).$$

Explicitly

$$F^t_{ij} = -t_{ij}\min(\left|k^t_{ij}\delta^t_{ij} - \eta^t_{ij}\delta^t_{ij}\right|, \mu\left|F^n_{ij}\right|). \quad (10)$$

Formally, the right-hand terms in Eq (5) present a composition of two independent torques. The contact torque (Fig. 8) with particle *j* is defined as vector product as originally proposed by Cundall and Strack (1979), namely:

$$T_{ij,cont} = d_{cij} \times F_{ij,cont}. \quad (11)$$

The second term in Eq (5) presents rolling resistance torque $T_{ij,\,res}$ which is introduced to account the non-spherical character of real particles. The latter may be interpreted as a frictional resistance torque defined in local plane:

$$T_{ij,\,res} = -\mu_r \left|F_n\right| R_i, \quad (12)$$

$$\mathrm{T}_{ij,cont} = \mathrm{d}_{cij} \times \mathrm{F}_{ij,cont}. \quad (13)$$

where F_n – the normal contact force; R_i – the min radius of the contacting spheres; μ_r – a rolling friction coefficient (Iwashita, Oda 2000).

4.2. Simulation and analysis

The numerical experiments were performed to investigate the behaviour of the soil specimen. Simulation capability is limited by a number of particles and lack of inter-particle data, therefore the several simplifications are introduced and applied for the current DEM simulations performed by *EDEM 2.2.1 Academic code. DEM solutions, 2009.*

Simulation of the full-scale sample would be enormously time consuming. Consequently, reduction of the problem size was done by reducing the size of computational domain. The cylinder of oedometric device was reduced seven times while retaining the ratio between height *H* and diameter *D*, i.e. $\frac{H}{D} = 0.5$. The reduced cylinder is defined by *H* = 5 mm and *D* = 10 mm. This simplification allows to retain the original scale of grains, while aspects ratio of cylinder and grain diameters is $\frac{D}{d} = \frac{10}{1.16} = 8.62$.

The data on particle physical properties of the investigated sand grains are defined indirectly. Different values of the density and the elastic constants for various modifications of silicon grains and may be found in available internet data sources and references.

Viscous damping effect is evaluated by a coefficient of restitution. The average value of the normal grain-wall coefficient of restitution $c^n_w = 0.5$ was obtained by the grain-bed collision experiments performed in the wind tunnel (Wang 2008) was taken for current simulations. This value was also employed for characterisation of the particle-particle interaction, thus the normal restitution coefficient magnitude is $c^n = 0.5$. This introduced assumption is mainly conditioned by the experimental difficulties arising in measurements of the grain-grain restitution. The tangential coefficient of restitution e^t is assumed to be fraction of the normal coefficient $e^t = \frac{e^n}{5} = 0.1$.

The role of friction of granular materials was reviewed by Zhu *et al.* (2007). Its influence on densification is emphasised here. It is obvious, that because of scattering of the experimental results (Horváth *et al.* 1996), only a rough approximation of the friction of sand is available. In many cases (Belheine *et al.* 2009; Oquendo *et al.* 2009; Rojek *et al.* 2005) various values of the friction coefficient between 0 and 1 are employed for numerical simulations. Here, the friction coefficient between the particle and wall (microscopic scale) is chosen to be the same, i.e. $\mu = \mu_w = \mu_{gr}$, while a relatively low value $\mu = 0.2$ is assumed regarding the smoothness of particles. The data values applied in the DEM simulations are summarized in Table 1.

Table 1. Major data on the sand particles

Quantity	Symbol	Value
Density, kg/m^3	ρ	2650
Elasticity modulus, GPa	*E*	73
Poisson's ratio	ν	0.17
Shear modulus, GPa	*G*	32
Tangential friction coefficient	μ	0.2
Rolling friction coefficient	μ_r	0.01
Normal coefficient of restitution	c^n	0.5
Tangential coefficient of restitution	c^t	0.1

Numerical simulation is naturally divided into two stages – generation of the initial state of particles, or packing stage and the compression stage.

Packing problem was comprehensively discussed in review paper of Zhu *et al.* (2007), packing of spheres in cylinder was discussed by Mueller (2005). The generation of cylindrical packing considered hereafter is subjected to specific requirements. Adequacy of the generated sample to the experimental one is retained by the specified value of the porosity e_0. From this the fixed volume of sand material in terms of the volume of grains V_{gr} is recalculated.

Another issue is the design of particles. In a case of the fractioned sample, diameters of particle are restricted by the specified min and max values d_{max} and d_{min}, respectively.

The initial state of the sample, i.e. location of particles in the cylinder, is obtained by the DEM, simulating the particle's deposition. Particle's diameters and placing above the cylinder are generated randomly. Later they fall

free due to the gravity force forming a packing structure. The process of filling was controlled by considering the evolution of the volume (or mass) particle and interrupted when it reaches specified values V_{gr} or m_{gr}, respectively. Finally, the total number N of particles is obtained.

As it was explained above, the dynamic state of particles at the time t is obtained by the numerical integration of the equations of motion (4–5). The explicit integration scheme with a constant time step Δt = 0.1 μs is applied. The magnitude of Δt is chosen to be a smaller than the Rayleight time step calculated by EDEM. The total time of filling t_f = 0.18 s is continued to stabilise of the particles motion after filling.

Two samples of the specimens composed of the coarse-sized and medium-sized grains were generated numerically. The characteristic data values for both specimens are summarized in Table 2.

Table 2. Data of the generated samples

Quantity	Symbol	Value	
		Sample 1	Sample 2
Initial porosity	e_0	0.740	0.814
Min particle diameter, mm	d_{min}	0.6	0.425
Max particle diameter, mm	d_{min}	1.16	0.6
Particles volume, cm^3	V_{gr}	0.2257	0.2165
Particles mass, g	m_{gr}	0.5981	0.5737
Number of particles	N	549	2993
Time step, μs	Δt	0.15	0.10
Rayleigh time step, μs	Δt_R	0.286	0.165
Simulation time of filling, s	t_f	0.28	0.28

The initial states of particles are shown in Fig. 9.

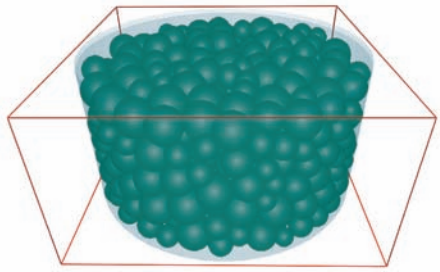

Sample 1

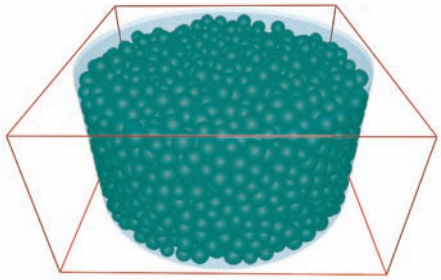

Sample 2

Fig. 9. Initial state of tested specimens

A simulation of compressing the specimens was performed in the second stage. It was realized in a slightly different manner comparing with the real experiment. Firstly, the compressive loading $p(t)$ was imposed by vertical moving the upper rigid wall of the cylinder with proportional increase of its vertical displacement $u_t(t)$. Secondly, the loading history was simplified by restricting to one stage load increment i.e. max load pressure 400 kPa was reached in shorter time without relaxation. An integration of the equations of motion (4–5) was performed with a constant time step, $\Delta t = 10^{-7}$ s.

The loading histories of both of the samples in terms of the top wall pressure $p(t)$ are given in Fig. 10. It could be observed that in Sample 1 with the coarse-grain particles, the max pressure $p_{max} = p(t_{L1})$ = 400 kPa was reached after t_{L1} = 1.08 s at the lower displacement $u_{max1}(t_{L1})$ = 0.076 mm ($\frac{\Delta h}{h}$ = 1.52%), while in Sample 2 with the medium-sized particles, the max pressure $p_{max} = p(t_{L2})$ = 400 kPa was reached after t_{L2} = 0.8 s at the lower displacement $u_{max2}(t_{L2})$ = 0.2 mm.

Compression results are presented in Fig. 11 in terms of the relationship between the porosity and pressure $e(p)$. Void ratio magnitudes are recalculated by expression (2) as $e(u_t(t))$, while pressures are taken from the DEM simulations. Here, DEM results are also compared to those being obtained experimentally (bold curve).

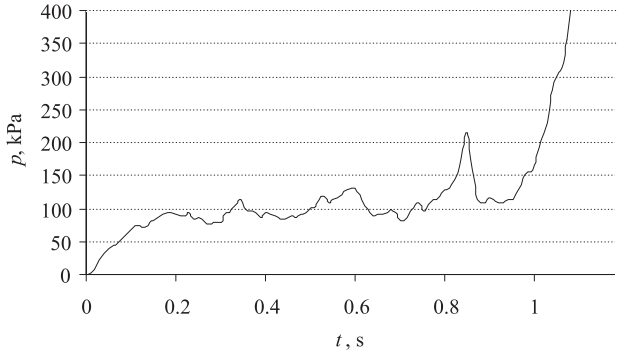

Sample 1

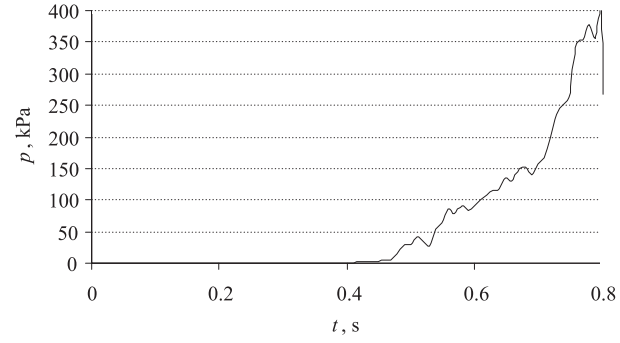

Sample 2

Fig. 10. Loading histories $p(t)$

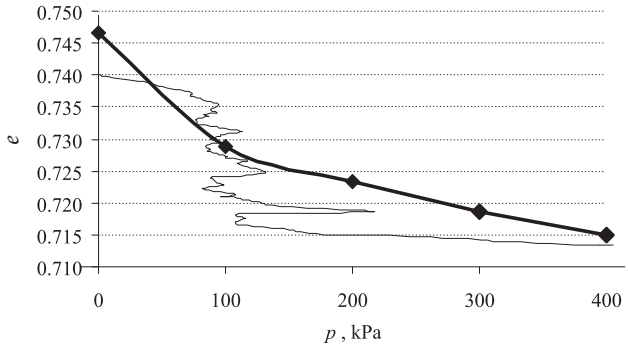

Fig. 11. Variation of the void ratio vs. pressure for Sample 1

5. Simulation results and discussion

A numerically simulated macroscopic behaviour in terms of pressure-displacement relationship contains descending intervals exhibiting instability of material. The above character is hardly to explain from the continuum point of view but we recognize it on the results of microscopic analysis of the particles motion.

Let us consider the central vertical section of Sample 1 (Fig. 12). The fragment of five red coloured particles is selected for analysis purposes. The central particle is denoted by capital letter C, while the four remainder particles by L (left), T (top), R (right) and B (bottom).

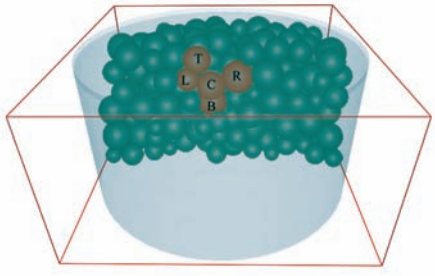

Fig. 12. Central vertical section of Sample 1 with marked particles

A motion of all selected particles during compression is characterized by velocity histories v_C, v_L, v_T, v_R and u_B (Fig. 13a). Particular velocity $v_i(t)$ stands for displacement magnitudes $v_i(t)=\sqrt{v_{ix}^2(t)+v_{iy}^2(t)+v_{iz}^2(t)}$. The relative motions of neighbour particles i with respect to the central particle C are characterized by differences of the velocity magnitudes $\Delta v_i(t)=v_i(t)-v_C(t)$ shown in (Fig. 13b). Comparing time instants of the pressure drop in (Fig. 10) it is easy to find that velocity-displacement jumps indicate the bifurcation from one dynamic equilibrium to the other.

6. Conclusions

Variation of the porosity of the Klaipėda sand during oedometric compression was investigated experimentally and by the Discrete Element simulations. Behaviour of separate (segregated) fractions and the whole mixture of the sand were treated independently.

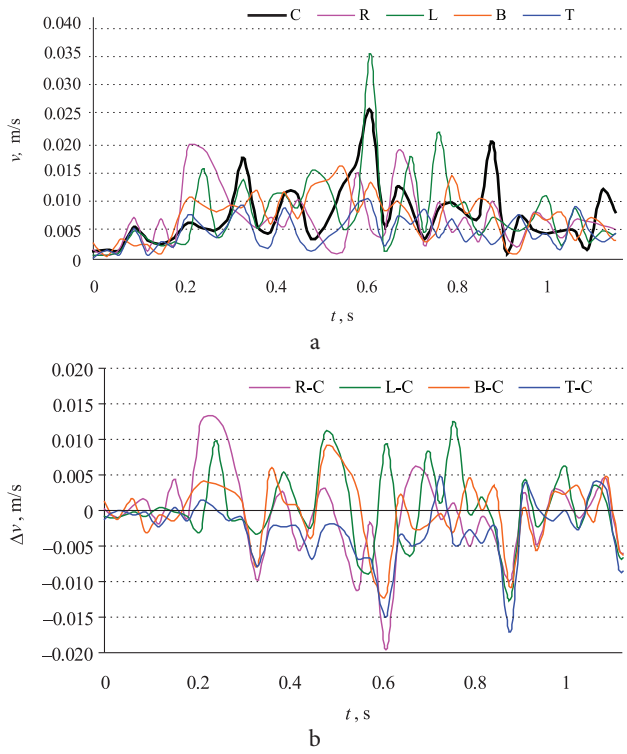

Fig. 13. Time histories of the absolute (a) and relative (b) displacements of the selected particles.

Porosity was characterised by the max (initial) and min (after compression) values of the void ratio. It was proved experimentally that porosity of the sand mixture with grain diameters ranging between 1.18 mm and 0.3 mm is characterised by max (e_0 = 0.844) and min (e_{04} = 0.714) values of the void ratio which are smaller compared to those of separate fractions. Moreover, these values are practically predicted by the coarse-grained fraction with grain diameters ranging between 1.18 mm and 0.3 mm.

DEM simulations confirmed generally the macroscopic experimental results and yielded additional data on microscopic behaviour. The non-smooth deformation behaviour was observed during detailed time-history analysis. The detected instabilities are explained by failure of microstructure and rearrangement of the sand grains.

Identification of the influence of other factors such as non-sphericity of particles, deformation rate, friction, etc., requires, however, the further research.

References

Allen, M. P.; Tildesley, D. J. 1987. *Computer Simulation of Liquids.* Oxford Science Publication. 408 p. ISBN: 0198556454

Amšiejus, J.; Dirgėlienė, N.; Norkus, A.; Žilionienė, D. 2009. Evaluation of Soil Strength Parameters via Triaxial Testing by Height versus Diameter Ratio of Sample, *The Baltic Journal of Road and Bridge Engineering* 4(2): 54–60. doi:10.3846/1822-427X.2009.4.54-60

Amšiejus, J.; Dirgėlienė, N. 2007. Probabilistic Assessment of Soil Shear Strength Parameters Using Triaxial Test Results, *The Baltic Journal of Road and Bridge Engineering* 2(3): 125–131.

Atkinson, J. H.; Clayton, C. R. I.; Head, K. H.; Ananostopoulos, A. G.; Bonnechere, F. 1997. *Incremental Loading Oedometer Test.* Document number: ETC5-D1.97.

Balevičius, R.; Džiugys, A.; Kačianauskas, R.; Maknickas, A.; Vislavičius, K. 2006. Investigation of Performance of Programming Approaches and Languages Used for Numerical Simulation of Granular Material by the Discrete Element Method, *Computer Physics Communications* 175(6): 404–415. doi:10.1016/j.cpc.2006.05.006

Belheine, N.; Plassiard, J. P.; Donzé, F. V.; Darve, F.; Seridi, A. 2009. Numerical Simulation of Drained Triaxial Test Using 3D Discrete Element Modeling, *Computers and Geotechnics* 36(1–2): 320–331. doi:10.1016/j.compgeo.2008.02.003

Cundall, P. A.; Strack, O. D. L. 1979. A Discrete Numerical Model for Granular Assemblies, *Geotechnique* 29(1): 47–65. doi:10.1680/geot.1979.29.1.47

Džiugys, A.; Peters, B. 2001. An Approach to Simulate the Motion of Spherical and Non-Spherical Fuel Particles in Combustion Chambers, *Granular Material* 3(4): 231–266. doi:10.1007/PL00010918

Fredlund, D. G.; Rahardjo, H. 1993. *Soil Mechanics for Unsaturated Soils*. Wiley-Interscience. 544 p. ISBN: 047185008X

Head, K. H. 1986. *Manual of Soil Laboratory Testing*, *vol. 3. Effective Stress Tests*. 2nd edition. London: Pentech Press, 422 p. ISBN-10: 0471977950

Horváth, V. K.; Jánosi, I. M.; Vella, P. J. 1996. Anomalous Density Dependence of Static Friction in Sand, *Physical Review E* 54(2): 2005–2009. doi:10.1103/PhysRevE.54.2005

Iwashita, K.; Oda, M. 2000. Micro-Deformation Mechanism of Shear Banding Process Based on Modified Distinct Element Method, *Powder Technology* 109(1–3): 192–205. doi:10.1016/S0032-5910(99)00236-3

Juknevičiūtė, L.; Laurinavičius, A. 2008. Analysis and Evaluation of Depth of Frozen Ground Affected by Road Climatic Conditions, *The Baltic Journal of Road and Bridge Engineering* 4(3): 226–232. doi:10.3846/1822-427X.2008.3.226-232

Kačianauskas, R.; Maknickas, A.; Kačeniauskas, A.; Markauskas, D.; Balevičius, R. 2010. Parallel Discrete Element Simulation of Polydispersed Granular Material, *Advances in Engineering Software* 41(1): 52–63. doi:10.1016/j.advengsoft.2008.12.004

Kruggel-Emden, H.; Simsek, E.; Rickelt, S.; Wirtz, S.; Scherer, V. 2007. Review and Extension of Normal Force Models for the Discrete Element Method, *Powder Technology* 171(3): 157–173. doi:10.1016/j.powtec.2006.10.004

Lade, P. V.; Prabucki, M. -J. 1995. Softening and Preshearing Effects in Sand, *Soils and Foundations* 35(4): 93–104.

Lade, P. V.; Wasif, U. 1988. Effects of Height-to-Diameter Ratio in Triaxial Specimens on the Behaviour of Cross-Anisotropic Sand, *Advanced Triaxial testing of Soil and Rock*. 1988, Philadelphia, USA. Philadelphia: ASTM STP 977, 706–714.

Marketos, G.; Bolton, M. D. 2010. Flat Boundaries and their Effect on Sand Testing, *International Journal for Numerical and Analytical Methods in Geomechanics* 34(8): 821–837. doi:10.1002/nag.835

Mitchell, J. K. 1993. *Fundamentals of Soil Behaviour.* 2nd edition. J. Wiley & Sons. 456 p. ISBN: 0471856401

Mueller, G. E. 2005. Numerically Packing Spheres in Cylinders, *Powder Technology* 159(2): 105–110. doi:10.1016/j.powtec.2005.06.002

Murthy, V. N. S. 2002. *Geotechnical Engineering: Principles and Practices of Soil Mechanics and Foundation Engineering.* CRC Press. 1056 p. ISBN: 0824708733

Oquendo, W. F.; Muñoza, J. D.; Lizcano, A. 2009. Oedometric Test, Bauer's Law and the Micro-Macro Connection for a Dry Sand, *Computer Physics Communications* 180(4): 616–620. doi:10.1016/j.cpc.2009.01.002

Ortigao, J. A. R. 1995. *Soil Mechanics in the Light of Critical State Theories.* Taylor & Francis. 160 p. ISBN: 9054101954

Peric, D.; Su, S. 2005. Influence of the End Friction on the Response of Triaxial and Plane Strain Clay Samples, in *Proc of the 16th International Conference on Soil Mechanics and Geotechnical Engineering*. 12–16 September, 2005, Osaka, Japan. Rotterdam: Millpress, 571–574.

Pöschel, T.; Schwager, T. 2004. *Computational Granular Dynamics: Models and Algorithms*. Berlin: Springer. 322 p. ISBN: 3540214852

Raji, A. O.; Favier, J. F. 2004. Model for the Deformation in Agricultural and Food Particulate Materials under Bulk Compressive Loading Using Discrete Element Method. I: Theory, Model Development and Validation, *Journal of Food Engineering* 64(3): 359–371. doi:10.1016/j.jfoodeng.2003.11.004

Rojek, J.; Zarate, F.; de Saracibar, C. A.; Gilbourne, C.; Verdot, P. 2005. Discrete Element Modelling and Simulation of Sand Mould Manufacture for the Lost Foam Process, *International Journal for Numerical Methods in Engineering* 62(11): 1421–1441. doi:10.1002/nme.1221

Terzaghi, K.; Peck, R. B.; Mesri, G. 1996. *Soil Mechanics in Engineering Practice.* 3th edition. NY: John Wiley & Sons. 592 p. ISBN: 0471086584

Tsuji, Y.; Tanaka, T.; Ishida, T. 1992. Lagrangian Numerical Simulation of Plug of Cohesionless Particles in a Horizontal Pipe, *Powder Technology* 71(3): 239–250. doi:10.1016/0032-5910(92)88030-L

Vervečkaitė, N.; Amšiejus, J.; Stragys, V. 2007. Stress-Strain Analysis in the Soil Sample during Laboratory Testing, *Journal of Civil Engineering and Management* 13(1): 63–70.

Wang, D.; Wang, Y.; Yang, B.; Zhang, W. 2008. Statistical Analysis of Sand Grain/Bed Collision Process Recorded by High-Speed Digital Camera, *Sedimentology* 55(2): 461–470. doi:10.1111/j.1365-3091.2007.00909.x

Yan, G.; Yu, H.-S.; McDowell, G. 2009. Simulation of Granular Material Behaviour Using DEM, *Procedia Earth and Planetary Science* 1(1): 598–605. doi:10.1016/j.proeps.2009.09.095

Zhu, H. P.; Zhou, Z. Y.; Yang, R. Y.; Yu, A. B. 2008. Discrete Particle Simulation of Particulate Systems: A Review of Major Applications and Findings, *Chemical Engineering Science* 63(23): 5728–5770. doi:10.1016/j.ces.2008.08.006

Zhu, H. P.; Zhou, Z. Y.; Yang, R. Y.; Yu, A. B. 2007. Discrete Particle Simulation of Particulate Systems: Theoretical Developments, *Chemical Engineering Science* 62: 3378–3392.

Ždankus, N. T.; Stelmokaitis, G. 2008. Clay Slope Stability Computations, *Journal of Civil Engineering and Management* 14(3): 207–212. doi:10.3846/1392-3730.2008.14.18

Received 28 January 2010; accepted 05 August 2010